Journal of the Atmospheric Sciences

Enhanced persistence of equatorial waves via convergence coupling in the stochastic multicloud model

--Manuscript Draft--

Manuscript Number:	
Full Title:	Enhanced persistence of equatorial waves via convergence coupling in the stochastic multicloud model
Article Type:	Article
Corresponding Author:	Noah Brenowitz New York University New York, NY UNITED STATES
Corresponding Author's Institution:	New York University
First Author:	Noah Brenowitz
Order of Authors:	Noah Brenowitz
	Yevgeniy Frenkel
	Andrew Majda
Abstract:	Recent observational and theoretical studies show a systematic relationship between tropical moist convection and measures related to large-scale convergence. It has been suggested that cloud fields in the column stochastic multicloud model compare better with observations when using predictors related to convergence rather than moist energetics (e.g. CAPE) \cite{Peters13}. Here, this work is extended to a fully prognostic multicloud model. A non-local convergence coupled formulation of the stochastic multicloud model is implemented without wind-dependent surface heat fluxes. In a series of idealized Walker cell simulations, this convergence coupling enhances the persistence of Kelvin wave analogs in dry regions of the domain while leaving the dynamics in moist regions largely unaltered. This effect is robust for changes in the amplitude of the imposed SST gradient. In essence, this method provides a \emph{soft} convergence coupling that allows for increased interaction between cumulus convection and the large-scale circulation, but does not suffer from the deleterious wave-CISK behavior of the Kuo-type moisture-convergence closures.
Suggested Reviewers:	Boualem Khouider khouider@math.uvic.ca
	Mitchell Moncrieff moncrief@ucar.edu
	George Craig George.Craig@dlr.de
	Karsten Peters Karsten.Peters@monash.edu

Click here to download Cost Estimation and Agreement Worksheet: Cost Estimation and Agreement Worksheet.pdf

Enhanced persistence of equatorial waves via convergence coupling in the stochastic multicloud model

Noah D. Brenowitz*, Yevgeniy Frenkel, and Andrew J. Majda

Department of Mathematics and Center for Atmosphere Ocean Science, Courant Institute of Mathematical Sciences, New York University, New York, NY

**Corresponding author address:* Department of Mathematics and Center for Atmosphere Ocean Science, Courant Institute of Mathematical Sciences, New York University, 251 Mercer St., New York, NY 10012, USA.

E-mail: noah@cims.nyu.edu

ABSTRACT

Recent observational and theoretical studies show a systematic relationship between tropical moist convection and measures related to large-scale convergence. It has been suggested that cloud fields in the column stochastic multicloud model compare better with observations when using predictors related to convergence rather than moist energetics (e.g. CAPE) (Peters et al. 2013). Here, this work is extended to a fully prognostic multicloud model. A non-local convergence coupled formulation of the stochastic multicloud model is implemented without wind-dependent surface heat fluxes. In a series of idealized Walker cell simulations, this convergence coupling enhances the persistence of Kelvin wave analogs in dry regions of the domain while leaving the dynamics in moist regions largely unaltered. This effect is robust for changes in the amplitude of the imposed SST gradient. In essence, this method provides a *soft* convergence coupling that allows for increased interaction between cumulus convection and the large-scale circulation, but does not suffer from the deleterious wave-CISK behavior of the Kuo-type moisture-convergence closures.

1. Introduction

Atmospheric dynamics in the tropics are characterized by the predominance of organized convection on a wide range of scales, spanning from mesoscale systems to synoptic and planetary-scale convectively coupled waves such as Kelvin waves and the Madden Julian oscillation (MJO) (Nakazawa 1974; Hendon and Liebmann 1994; Wheeler and Kiladis 1999). Despite continued efforts by the climate community, present coarse resolution General Circulation Models (GCMs) poorly represent variability associated with tropical convection (Slingo et al. 1996; Moncrieff and Klinker 1997; Scinocca and McFarlane 2004; Lau and Waliser 2005; Zhang 2005). One of the main sources of error in these models arises from deficiencies in the treatment of cumulus convection (Moncrieff and Klinker 1997; Lin et al. 2006), which has to be parameterized in coarse resolution GCMs. However, marked improvement have been made in a few GCM simulations recently (Khouider et al. 2011; Del Genio et al. 2012; Crueger et al. 2013; Deng et al. 2014; Ajayamohan et al. 2013, 2014). Given the importance of the tropics for climate prediction and numerical weather prediction (NWP), the search for new strategies for parameterizing the unresolved effects of tropical convection has been a key focus of researchers during the last few decades.

Several methods have been developed to address the multiscale nature of the problem. Cloud-resolving models (CRM) on fine computational grids as well as high-resolution numerical weather prediction (NWP) models with improved convection parameterizations have succeeded in representing some aspects of organized convection (ECMWF 2003; Moncrieff et al. 2007; Slawinska et al. 2014b). In addition, superparameterization (SP) methods (Grabowski and Smolarkiewicz 1999; Grabowski 2001, 2004; Randall et al. 2003; Majda 2007) and sparse space-time SP (Xing et al. 2009; Slawinska et al. 2014a) use a cloud resolving model in each column of a large-scale GCM to explicitly represent small scale processes, mesoscale processes and interactions between them. However, these methods are not currently computationally viable for application to large ensemble weather prediction or climate simulations. Thus, the search for computationally inexpensive and realistic convection parameterizations that are seamlessly scalable between medium and coarse resolution GCMs remains a central unsolved problem in the atmospheric community (Arakawa 2004).

A closely related issue to the parameterization problem is the development of theories relating cumulus convection and the large scale variables. An early theory for this cross-scale interation is the Convective Instability of the Second Kind (CISK) idea (Charney and Eliassen 1964). CISK describes a two way feedback between cumulus convection and wind convergence in the planetary boundary layer. In the original formulation, this convergence is caused by Ekman pumping due to the large scale geostrophically balanced circulation, but wave-CISK is a theory which is more relevant to non-balanced equatorial flows (Lindzen 1974).

Both forms of CISK are heavily criticized in the literature in favor of an alternative known as the Quasi-Equilibirum (QE) hypothesis (Arakawa and Schubert 1974; Emanuel et al. 1994; Arakawa 2004). In the broadest sense, QE supposes that over large spatial scales cumulus convection acts to remove static instability in an atmospheric column. The static stability is typically a functional of the humidity and temperature fields; therefore, for the present purposes, we define a QE parameterization as any scheme that relates total precipitation to the humidity and temperature alone. In the QE context, the hypothesis of wind induced surface heat exchange (WISHE) provides a mechanism for the interaction between the large-scale circulation and cumulus convection (Emanuel et al. 1994). While this mechanism is well-established for tropical cyclones, it is unclear to what extent WISHE is relevant to dynamics in equatorial regions (Grabowski and Moncrieff 2001).

For each of the physical hypotheses above, there is a corresponding set of operational cumulus parameterations. Broadly speaking, convection schemes can be divided into those based on moisture-convergence closures (Kuo 1974), the moist adjustment idea (Manabe et al. 1965), and the Quasi-equilibrium (QE) hypothesis(Arakawa and Schubert 1974; Betts and Miller 1986). CISK thinking informed the moisture-convergence schemes. The QE hypothesis at its core is a statement about statistical equilbrium, but the atmosphere in reality is far from equilibrium. Moreover, the QE hypothesis breaks down as the current GCM grid sizes approach the cumulus scale. One generic design principle for treating nonequilibrium systems in atmosphere ocean science is the addition of stochastic perturbation (Buizza et al. 1999; Palmer 2001; Lin and Neelin 2003; Khouider et al. 2003; Majda et al. 2008; Majda and Stechmann 2008). In particular, one of the more promising approaches has been the use of Markov-chain lattice models to represent unresolved sub-grid variability (Khouider et al. 2003). This type of lattice model is an extension of an Ising spin-flip model used for phase transitions in material science (Majda and Khouider 2002; Katsoulakis et al. 2003b), and has been successfully used to improve simple convection parameterizations (Khouider et al. 2003; Majda et al. 2008; Khouider et al. 2010; Frenkel et al. 2012, 2013. Another stochastic cumulus convection parameterization is that of (Plant and Craig 2008).

In addition to stochastic parameterization, there have been large improvements in deterministic parameterizations. Some drivers of these improvements include large field campaigns such as the TOGA-COARE (Moncrieff and Klinker 1997) and an enhanced understanding of organized convection. In particular, a clearer understanding of equatorial convectively coupled waves (Wheeler and Kiladis 1999; Kiladis et al. 2009; Straub and Kiladis 2002) has informed the development of the multicloud parameterizations (Khouider and Majda 2006b,a, 2007, 2008a,b; Khouider et al. 2010; Frenkel et al. 2012). The multicloud parameterizations take advantage of the observed self similarity and vertical structure of equatorial waves (Wheeler and Kiladis 1999), and have been successfully blended with the Ising model stochastic parameterization approach (Frenkel et al. 2012, 2013) (hereafter FMK13 and FMK13). Moreover, both the deterministic and the stochastic multicloud model (SMCM) can realistically replicate aspects of convectively coupled waves and intraseasonal oscillation in a prototype GCM setting (Khouider et al. 2011; Deng et al. 2014; Ajayamohan et al. 2013, 2014).

In this study, we revisit the controversy between CISK and QE, motivated by recent work with observations from Darwin, Australia that has established a strong link between the large scale convergence field and local convection (Davies et al. 2013). Moreover, this study failed to find a strong link between CAPE and local precipitation. Motivated by these observations, several studies have attempted to infer causality by fitting multicloud-based stochastic models to the estimated cloud fraction fields (Peters et al. 2013; Dorrestijn et al. 2015; Chevrotière et al. 2014). They found that large-scale pressure velocity at 500hPa from a reanalysis product is a better predictor of convection over Darwin than the corresponding moist thermodynamic state. These data have also been used to evaluate several operational convective mass-flux trigger functions (Suhas and Zhang 2014). Moreover, there is evidence that the transition from shallow to deep convection is linked to the large scale vertical moisture advection (Hagos et al. 2014 and references therein).

The studies above are based on based on diagnostics from a single location, but the idea of convergence-coupling has been primarily criticized on a dynamical basis (Emanuel et al. 1994). To address these concerns, the aim of this paper is to develop a prototype non-local stochastic convection parameterization that takes into account the effects of large-scale convergence and avoids the pitfalls of conventional moisture-convergence closures (Kuo 1974). The primary aim here is to explore the dynamical consequences of this additional physical assumption. Because the SMCM shows realistic variability in computationally inexpensive one dimensional simulations (Frenkel et al. 2013), it is an idea test bed for these ideas. There has also been some recent work on implementing the SMCM with convergence coupling in the ECHAM GCM (Peters et al. 2015).

Specifically, a flexible framework for including the effects of convergence coupling in the SMCM is developed. Using this framework, it is shown that coupling the interaction of congestus and deep clouds to the large scale convergence leads to realistic variability. This approach blends the convergence-coupling idea with the CAPE-coupling approach used in past work (Khouider and Majda 2006a,b, 2008a,b;FMK12,13). In some respects, the non-local convergence coupling introduced here accounts for non-local interactions between microlattice convective sites, and it complements recent work along these lines (Khouider 2014).

In the present paper, we find that in spatially extended idealized Walker cell simulations, this deep-convergence-coupled SMCM shows an overall increase in variability about the mean and an enhanced low frequency variability. In particular, the coupling enhances the persistence of moist gravity waves in the dry regions flanking the central warm-pool. These waves have an approximate phase speed of 10 m/s and significantly warm and dry the atmosphere in their wake. There is observational evidence that Kelvin waves do indeed propagate with remarkable persistence across planetary zonal distances (Kiladis et al. 2009; Straub and Kiladis 2002; Wheeler and Kiladis 1999).

Moreover, an intermittent regime-switching behavior arises on intraseasonal time scales that switches the system between epochs of regular and irregular walker cell variability as seen in CRM simulations (Slawinska et al. 2014a,b). However, these benefits are only conferred when the transition of congestus to deep convection is convergence coupled. Naively replacing the model's implicit low-level moisture convergence coupling with an explicit dry convergence coupling leads to degeneracies, such as extreme sensitivity to numerical resolution. Gains from convergence coupling only occur when modelling the formation of deep rather than shallow clouds. This is consistent with observations (Davies et al. 2013).

The paper is outlined as follows. In Section 2, two prototype parameterizations are developed which, respectively, couple congestus and deep clouds to the large scale convergence. Then, Section 3 describes the setup for the idealized Walker circulation experiments. Results for the schemes are shown in Section 4. Particular attention is given to the deep-convergence-coupled results in Section 4a, and the degenerate congestus-convergence-coupled scheme in Section 4b. Concluding remarks are given in Section 5.

2. Stochastic Multicloud model

The multicloud model (Khouider and Majda 2006b,a, 2008b) and its stochastic variant (FMK12,13; Khouider et al. 2010; Deng et al. 2014) have been successful in replicating the observed dynamics of organized tropical convection by coupling heating rates to the large scale thermodynamic state. As hinted in the introduction, the SMCM does this by capturing stochastic transitions between congestus, deep, and stratiform cloud sites (FMK12,13;Khouider et al. 2010) as seen in Figure 1. It accomplishes this via a computationally-efficient coarse-grained continuous time Markov chain for the fraction of congestus σ_c, deep σ_d, and stratiform σ_s sites in a given numerical grid cell (Katsoulakis et al. 2003b,a; Khouider and Majda 2008b). Like the CIN model, this setup distinguishes between the processes that lead to the formation of convection sites from those which alter the magnitude of the heating. Therefore, stochastic convergence-coupling does not necessarily entail a wave-CISK type instability in the SMCM.

The SMCM also allows for realistic physically-motivated interactions between cloud types which are easily coupled in a explicit fashion to any deterministic quantity of choice. Using such a model we can hope to address the validity of the convergence-coupling hypothesis. As such, extending the work of (Peters et al. 2013) to the prognostic spatially-extended SMCM provides an ideal test-bed for gauging the validity of the convergence coupling hypothesis in state-of-the-art convection schemes.

Along these lines, Section 2a contains abbreviated description of the two baroclinic-mode dynamical core. The stochastic coupling to the large-scale thermodynamics and convergence is introduced in Section 2b.

a. Dynamical core and convection closure

(Khouider and Majda 2006b,a, 2008b; Khouider et al. 2010; FMK12,13) assume three heating profiles associated with the main cloud types that characterize organized tropical convective systems (Johnson et al. 1999): cumulus congestus clouds that heat the lower troposphere and cool the upper troposphere through radiation and detrainment, deep convective towers that heat the whole tropospheric depth, and the associated lagging-stratiform anvils which heat the upper troposphere and cool the lower troposphere due to evaporation of stratiform rain. In its simplest form, the multicloud model captures these three modes of heating using the first two vertical modes of a constant stratification Boussinesq system. Therefore, the simplest version of the dynamical core of the multicloud parameterizations consists of two coupled and forced shallow water systems. To simplify the current study, the meridional dependence of the equations is ignored, and the simulations are performed in a single ring of latitude. In CRM simulations (Slawinska et al. 2014b) and the past work on the multicloud model, this one dimensional setup has proved sufficient to generate a wide array of interesting variability. This is especially true in simulations with a non uniform SST pattern.

The deterministic equations and closures are identical to FMK13, so we simply summarize them here. For more details and intuition, see FMK13 and references therein. The equations for the prognostic deterministic variables are given by

$$\frac{\partial u_1}{\partial t} - \frac{\partial \theta_1}{\partial x} = C_d u_0 u_1 - \frac{1}{\tau_R} u_1 \tag{1}$$

$$\frac{\partial u_2}{\partial t} - \frac{\partial \theta_2}{\partial x} = C_d u_0 u_2 - \frac{1}{\tau_R} u_2 \tag{2}$$

$$\frac{\partial \theta_1}{\partial t} - \frac{\partial u_1}{\partial x} = P - \mathrm{Rad}_1 \tag{3}$$

$$\frac{\partial \theta_2}{\partial t} - \frac{1}{4}\frac{\partial u_2}{\partial x} = H_c - H_s - \mathrm{Rad}_2 \tag{4}$$

$$\frac{\partial \langle q \rangle}{\partial t} + \frac{\partial}{\partial x}\langle uq \rangle = -\frac{2\sqrt{2}}{\pi} P + \frac{D}{H_T} \tag{5}$$

$$\frac{\partial \theta_{eb}}{\partial t} = \frac{1}{h_b}(E - D) \tag{6}$$

$$\frac{\partial H_s}{\partial t} = \frac{1}{\tau_s}(\alpha_s \sigma_s H_d / \bar{\sigma}_d - H_s). \tag{7}$$

The velocity (u_j) and potential temperature (θ_j) equations are derived in standard fashion by Galerkin projection of the rigid-lid dry Boussinesq equations onto the first two baroclinic modes $Z(z)$ and $Z(2z)$, where $Z(z) = \sqrt{2}\cos(\pi z / H_T)$ for $0 \leq z \leq H_T$.

The column integrated moisture ($\langle q \rangle$) equation is relatively straightforward. The main difficulty is showing that the column integrated moisture flux can be approximated by

$$\langle uq \rangle = (u_1 + \tilde{\alpha} u_2)\langle q \rangle + \tilde{Q}(u_1 + \tilde{\lambda} u_2),$$

which is shown in Appendix A of (Khouider and Majda 2006b). This moisture flux includes linear and nonlinear constributions from the first and second baroclinic velocities, and includes the familiar gross moist stability $\tilde{Q}$ as a parameter (Frierson et al. 2004).

The boundary layer equivalent potential temperature (θ_{eb}) is forced convective downdrafts D and the evaporation E, and has no advective contributions linear or otherwise. The multicloud formulation enters through the three heating rates H_c, H_d, and H_s which represent congestus, deep, and stratiform convective heating, respectively. These and other important diagnostic quantities are given in Table 2.

The reader will note that the heating rates H_d and H_c are each the product of cloud fraction fields σ_d and σ_c and some measure of the energy available for convection. The energy available for congestus and deep heating are distinct but closely related quantities that depend only on the thermodynamic degrees of freedom θ_{eb}, q, θ_1, and θ_2. While diagnostic closures adequately model congestus and deep heating, FMK13 showed an improvement when using lag differential equation to model the stratiform heating, and this is the form used in (7). On the other hand, the cloud fractions fields are treated as stochastic processes that evolve according to a set of intuitive rules described in the next section (Khouider et al. 2010; FMK12,13).

b. Stochastic coupling

The evolution of the cloud fractions is given by a continuous time Markov-chain which has transition rates that depend on the large-scale variables of the system. This approach to stochastic parameterization is introduced in (Majda and Khouider 2002; Khouider et al. 2003), and can be roughly thought of as introducing a state-dependent multiplicative "noise". However, because the Markov-chain is defined on a discrete state-space, the simulated pathways cannot be described using an Langevin equation with white-noise (Gardiner 2009).

The stochastic parameterization attempts to model sub grid-scale dynamics explicitly by defining a lattice within each coarse grid cell. The underlying PDE ((1)-(7)) is discretized onto a regular numerical mesh, and each grid cell is further divided into a rectangular $\ell \times \ell$ lattice. Each element of this lattice is occupied by either a congestus, deep, or stratiform cloud or by a clear-sky site, which are represented respectively by the integers 1, 2, 3, and 0 (clear-sky). A continuous time Markov-chain, that allows for transitions between these four states at a certain rate is defined on this discrete state-space. These sorts of models have been used in material science and chemistry to model the reaction of different chemical species (Gillespie 1977), but the approach here is to couple the transition rates between clouds to a PDE ((1)-(7)) via the large-scale resolved variables.

The SMCM allows for a few different transitions between the cloud types. With the associated transition rate in parenthesis, these transitions are:

1. Formation of a congestus cloud from clear sky (R_{01})

2. Formation of a deep cloud from clear sky (R_{02})

3. Conversion from a congestus to a deep cloud (R_{12})

4. Conversion from a deep to a stratiform cloud (R_{23})

5. Decay of congestus (R_{10}), deep (R_{20}), or stratiform clouds. (R_{30})

In (FMK12,13), these transition rates depend only on the large-scale thermodynamic quantities so that

$$R_{ij} = R_{ij}(q, \theta_{eb}, \theta_1, \theta_2), \quad i, j \in [0, 1, 2, 3]$$

The precise details of these formula are constrained by a set of intuitive rules which are based on observations of cloud dynamics in the tropics (e.g. Johnson et al. 1999; Mapes 2000; Khouider and Majda 2006b, and references therein). In general, moisture and θ_{eb} will tend to promote active convection, and high tropospheric temperatures will tend to discourage it.

The present study concludes that the conversion from congestus to deep (R_{12}) is the critical transition for convergence coupling. However, more generally, a modification can be introduced so that

$$R_{ij} = R_{ij}(q, \theta_{eb}, \theta_1, \theta_2, W_{ij}) \tag{8}$$

where W_{ij} is a proxy which depends on the large-scale convergence.

c. Transition rates with convergence coupling

Before delving into the definition of W_{ij} in (8), it is useful to note the precise form of the vertical velocity w in any two baroclinic mode Boussinesq model. Mass continuity requires that w at a height z be given by

$$w = -\int_0^z \nabla \cdot \mathbf{u} dz' = \nabla \cdot \mathbf{u}_1 Z'(z) + \frac{1}{2} \nabla \cdot \mathbf{u}_2 Z'(2z), \tag{9}$$

where $Z(z) = \sqrt{2}\cos(\pi z/H_t)$ is as given in the previous section.

As mentioned before, convergence coupling is traditionally seen as providing a mechanism for interactions between the convective and large scale motions. The radius over which this interaction occurs should be a parameter of the convection scheme rather than a function of the grid size. Simply evauluating the *grid-scale* convergence using centered differences will not be sufficient because the differencing implicitly depends on the grid-size. This effect is ameliorated by averaging the *grid-scale* convergence over a given "interaction" radius R. Specifically, the *large-scale* convergence for given location and height is given by

$$W^R(x,z) = \frac{1}{2R} \int_{x-R}^{x+R} w dx = Z'(z) \Delta_R u_1 + \frac{1}{2} Z'(2z) \Delta_R u_2, \tag{10}$$

with the backward centered difference operator $\Delta_R f = (f(x-R) - f(x+R))/2R$. This approach also allows reasonable comparison between models with different grid sizes. With this machinery in hand, it is possible to pose the transition rates for the stochastic process.

In general, the convergence coupling will effect the formation of deep clouds, formation of congestus clouds, and the transition between the two. We currently do not include any convergence coupling for the decay of clouds or the formation of stratiform clouds, but this is a potential topic of future research. With these physical assumptions, the general formulation of the convergence coupled transition rates is given by

$$R_{01} = \frac{1}{\tau_{01}}\Gamma(C_l)\Gamma(D)\Gamma(W_{01}) \tag{11}$$

$$R_{12} = \frac{1}{\tau_{12}}\Gamma(C)(1-\Gamma(D))\Gamma(W_{12}) \tag{12}$$

$$R_{02} = \frac{1}{\tau_{02}}\Gamma(C)(1-\Gamma(D))\Gamma(W_{02}) \tag{13}$$

where $\Gamma(x) := 1-\exp(-x)$. $\Gamma(x)$ is designed to normalize the tendency of each factor and satisifies $0 < \Gamma(x) \leq 1$. The only difference between these rates and those of FMK13 is the additional factor $\Gamma(W_{ij})$. The other transitions are left unaltered, and a comprehensive list of the transition rates is available in Table 3.

The convection propensities W_{01}, W_{12}, and W_{02} represent the large scale convergence evaluated at the vertical level relevant to the transition. Specifically,

$$W_{ij}(x) = \overline{W} + \tau_w \cdot \left[W^R(x, z_{ij})\right]^+, \tag{14}$$

where z_{ij} is the vertical level governing the transition, τ_W is the strength of the convergence coupling, and $\overline{W}$ is a constant mean propensity for convergence. Here, we assume that the formation of congestus clouds, the formation of deep clouds, and the transition from congestus to deep clouds occur in order of increasing height. In all cases, these heights are within the free troposhere and generally include a contribution from both the first and second baroclinic convergence fields. For a schematic view of the covergence coupled stochastic multicloud model see Figure 1. For completeness, Table 1 contains a comprehensive list of parameters which includes parameters from FMK13 as well as the newly introduced convergence coupling parameters.

In the formulation above, R_{01} R_{02}, and R_{12} each involve the product of three different factors (cf. Tab. 3). One factor $\Gamma(W_{ij})$ is related to the large scale convergence, while the other two are related to the grid-scale thermodynamics. This setup is general, but it is not clear that all three transitions considered in (11)–(13) should be coupled to the large-scale convergence simultaneously. To address this ambiguity, this paper will study three different kinds of stochastic setups.

1) THERMODYNAMICS-ONLY COUPLING (THERMO)

A thermodynamics-only setup is a base case for that yields results that are nearly identical to FMK13. This setup is obtained by setting $\tau_w = 0$ which implies that $W_{ij} = \bar{W}$ a constant value.

2) CCON CONVERGENCE COUPLING (CCON)

Another possible setup is one that couples the formation of congestus clouds to the large scale convergence alone. In FMK13 and other works (Khouider and Majda 2006a,b; Khouider et al. 2010), it is shown that the thermodynamic-only SMCM already features an implicit low-level moisture convergence mechanism resulting from second-baroclinic contribution to (5) and the moisture-dependence of C_l. Wholesale replacing this *implicit* moisture-convergence mechanism with an *explicit* dry-convergence coupling fundamentally alters the underlying cloud formation mechanism of the SMCM, and provides an interesting albeit unrealistic test-bed for the convergence-coupling idea. The CCON setup yields intriguing improvements for some parameter regimes, but, as expected, suffers from extreme sensitivity to these same parameters.

In particular, this setup fixes $W_{02} = W_{12} = \overline{W} = -\log(.99)$ and $C_l = \bar{C}$.

3) DEEP CONVERGENCE COUPLING (DCON)

These degeneracies are not present when the transition from congestus to deep clouds is coupled to the large-scale convergence. As will be seen in subsequent sections, this DCON stochastic setup allows for the benefits of the THERMO simulations while altering the dynamics of large scale convectively coupled waves in a realistic and intriguing fashion. The DCON setup consists of fixing $W_{01} = W_{02} = \overline{W} = -\log(.8)$ while allowing C, C_ℓ, and W_{12} to vary.

3. Idealized Walker circulation simulations

The past work on convergence coupling is typically focused on its role mediating interactions between convection, tropical cyclones (Charney and Eliassen 1964), and synoptic scale equatorial waves (Lindzen 1974). Therefore, we expect the convergence coupling designed here to show interesting characteristics in simulations with an imposed large scale circulation. In the SMCM, a planetary-scale SST pattern that mimics the so-called Indonesian "warm pool" will force an idealized version of the Walker circulation. This is a standard test bed for simplified convection parameterizations (Khouider et al. 2003; FMK13).

Because there is no surface sensible heat flux in the SMCM, the only impact of elevated SST is through the evaporation term (c.f. Table 2). The sea surface saturation equivalent potential temperature for a warm pool simulation takes the form

$$\theta^*_{eb}(x) = A_{SST}\cos\left(\frac{4\pi x}{40000}\right) + 10K, \tag{15}$$

within an interval of 20,000 km of the 40,000 km domain, and $\theta^*_{eb} = 10 - A_{SST}$ elsewhere as in (Khouider and Majda 2006b, 2008b; FMK12,13). Unless otherwise stated $A_{SST} = 5$K. This setup mimics the Indian Ocean-Western Pacific warm pool, and has yielded interesting Walker-like circulations in FMK13.

Time series of 1000 days are generated for each formulation of the transition rates, using a time step of 30 seconds and a total of 1000 grid cells spread over a 40,000 km equatorial domain. The number of stochastic elements per coarse grid cell is $\ell^2 = 30^2 = 900$. Unless otherwise stated, the convergence coupling strength is fixed at $\tau_w = 10$ hr, and the interaction radius is fixed at $R = 240$ km. These and other parameters are given in Table 1.

The numerical method used here is same as that used in FMK13. Namely, an operator splitting strategy is used which alternates solutions of the hyperbolic terms, source terms, and stochastic process. The conservative terms are discretized and solved by a non-oscillatory central differencing scheme while the remaining deterministic forcing terms are handled by a second-order Runge-Kutta method (Khouider and Majda 2005a,b). The stochastic component of the scheme is resolved using Gillespie's exact algorithm (Gillespie 1975). For more details on the algorithm see (Khouider et al. 2010; FMK12,13).

Here, we note that combining convergence-coupling for the congestus *and* deep transitions invariably results in a strong numerical instability for reasonable values of Δt and τ_w. This is why we only consider the CCON and DCON stochastic setups, rather than some combination of the two.

4. Results

First, we will provide a qualitative overview of the dynamics of the three stochastic setups. The anomalies from the temporal mean of the first baroclinic velocity (u_1) for THERMO, DCON, and CCON are available in Figure 2, and the corresponding climatological mean and variance are shown in Figure 3.

All stochastic setups show interesting variability about the mean, but the nature of the variability is subtly altered between the simulations. All three simulations show small-scale wave activity in the center of the domain (e.g. the high SST region), corresponding to a background of convective activity. However, the simulations differ in the behavior of large convectively coupled waves (CCWs) at the edges of the elevated SST region. The THERMO simulation has the same behavior as previously seen in (FMK12,13) with strong second-baroclinic heating around 20,000 km which transitions to deep heating in the form of CCWs around 25,000 km (not shown). In the u_1 field, the most salient feature is the strong and regular convectively coupled waves that depart the warm-pool region every 12 days in strictly alternating order.

Adding convergence coupling to either the congestus (CCON) or deep (DCON) transitions, results in breakdown of this order. The CCON regime represents a more drastic alteration and features strong CCWs on many different scales interacting with each other without the emergence of a clear periodicity. The DCON regime provides a more subtle alteration that causes the regular waves to leave the warm-pool at double the period (24 days) and to propagate further into the dry region. Occasionally, one of these waves will circle the domain entirely to re-interact with the warm-pool as can be seen around day 930. This interaction initiates a transition to a more chaotic regime for long periods of time. This *enhanced persistence* of the CCWs is the primary result of this study.

The simulations have a roughly comparable mean u_1 climatology (6 m/s) except for the CCON simulation, which has a peak mean u_1 of ~ 4 m/s. On the other hand, the second baroclinic u_2 structure changes substantially between the simulations. While the DCON setup is quite similar to the base case THERMO setup, the CCON simulation does not feature the characteristic double-peak in the second baroclinic velocity component.

The total variability about the mean also differs subtly between the setups. The THERMO and DCON schemes show a triple peaked variability structure that is due to a triple peak in convective heating seen in past results (FMK12,13). On the other hand, the CCON setup shows larger variability throughout the domain, but with a much flatter peak . However, as will be shown later, the CCON setup is degenerate and extremely sensitive to parameters, and we emphasize that it is important to favor *realistic* over larger variability.

a. Deep convergence coupled DCON

In the formulation above, two key parameters were introduced: R and τ_w. Of these two, the parameter τ_w explicitly tunes the strength of the convergence coupling through Eq. 14, while R has a more subtle effect. In this section, we study the effect of varying τ_w, which we will often refer to as the "convection strength" or "strength parameter", in the context of the deep-convergence-coupled DCON simulations. In particular, we perform simulations fixed at $R = 240$ km and for $\tau_w = 0,\ 1,\ 10,\ 100$, and 1000 hr. Of course, $\tau_w = 0$ implies that the convergence coupling is disabled, which is the same as the THERMO setup following (14).

This deep-convergence-coupled setup shows improved low-frequency variability and intermittent dynamics as is readily visible in the anomalous u_1 Hovmoller diagrams shown in Figure 4. From left-to-right with increasing τ_w, the Hovmoller diagrams represent a continuum from order to disorder. As discussed in the previous section, the majority of the variability in the thermodynamics-only (THERMO) simulation ($\tau_w = 0$) is comprised of large CCWs that emanate from the warm-pool region at regular $\sim$12 day intervals. Moreover, these CCWs alternatively propagate eastwards and then westwards in perfect sequence. For $\tau_w = 1$, this structure is still somewhat visible, but the coherence and regularity of these waves is weakened. With $\tau_w = 10$, large CCWs similar to those in THERMO, but with a 2x longer time scale, alternatively propagate east/west until one circles the domain and interacts once more on the warm-pool region (see day 930). This interaction then initiates a series of many small and large CCWs, which are released from the center of the domain. This behavior is markedly more chaotic and features variability on longer time scales then the regular east-then-west waves in the THERMO. The effect is increasingly pronounced for $\tau_w = 100$ and 1000.

The u_1 climatology shown in upper panel of Figure 5 reflects this increased variability outside the warm-pool region. While the mean fields of the convergence-coupled simulations do show a slightly stronger circulation between 15,000 km and 25,000 km, the result is quite subtle. On the other hand, there is a large increase in variability with τ_w, especially outside of the warm-pool region. This is evidently due to the propagating CCWs visible in Figure 4.

1) ENHANCED PERSISTENCE OF EQUATORIAL WAVES

In this section, we present qualitative and quantitative evidence for the enhanced persistence of the CCWs in the regions between 25000 and 35000 km and between 5000 and 15000 km. We will hereafter refer to these regions as the "flanks" of the warm-pool.

The large CCWs in the flank regions of the convergence-coupled simulations have an interesting phase speed and wave structure. Figure 6 shows a zoomed-in Hovmoller diagram of one such example in the $\tau_w = 10$ simulation. The wave is generated in the warm pool, and—as it propagates eastward—its phase speed is reduced when it exits the warm pool region around 25,000 km. Moreover, the wave appears to be partially sustained by reciprocal interactions with the warm-pool via fast-moving gravity waves. This is a consequence of the convergence-coupling which enables the interaction of dry-waves with moist-waves. The dynamical fields are averaged along the traveling wave in the two marked segments and the resulting wave structure is plotted in Figure 7. As the wave leaves the warm pool and slows, it transitions from congestus-dominated to deep-dominated heating. This occurs because the available energy in the dry region for congestus convection is much lower than that available for deep convection.

The persistence of these waves can be quantified using the lagged correlation structure of the data. From Figure 7, it is clear that the signature of the large CCWs in the flank regions is an efficient conversion from congestus heating (H_c) to deep heating (H_d). This effect can be quantified by seeing how well H_c for a particular spatial location x_0 predicts H_d in other spatial locations. In particular, the diagnostic we use is the lagged correlation function given by

$$\rho(x,\tau;x_0) = \mathrm{Corr}(H_c(x_0,t), H_d(x,t+\tau)). \tag{16}$$

To identify waves propagating the in the flank regions, a seed location of $x_0 = 30,000$ km is used. The results for the THERMO and DCON simulations are available in Figure 8. These plots are quite similar to the Hovmoller diagrams shown in Figure 3 and 4, but filter for CCWs in the flank region and represent an average over many individual wave events. For both THERMO and DCON, the large CCW near the x_0 is clearly visible as a line of high correlation coefficients that extends towards the center of the domain. In the THERMO simulation, the waves appear to dry and decohere around the seed of $x_0 = 30,000$ km. For the DCON simulation, these waves propagate with the same phase speed for an additional 7 days until the correlations vanish around 35,000 km. Because this result is an average over all flank region CCWs and provides a quantitative confirmation of the qualitative results in Figures 4 and 6.

Another interesting consquence of the convergence coupling is that it appears to reduce long distance lagged correlations. In the THERMO results, the seed location strongly correlates with a wave around 15000 km on the other side of the warm pool. This is likely because the flank region CCWs in the THERMO scheme are much more strongly linked to convective activity in the warm pool region between 15000 km and 25000 km. There are no similar long distance correlations in the DCON scheme, so the DCON scheme appears to discourage this link. Put another way, convergence coupling encourages interaction with local atmosphere in the flank regions, rather than slaving it to the convective activity in the warm pool.

2) Sensitivity to SST gradient

A simple way to enhance persistence in an idealized Walker cell simulation is to make the dry regions moister by reducing the amplitude of the imposed SST pattern. Here, this is accomplished by reducing A_{SST} from 5 to 4.5 K, which amounts to a 1 K reduction in the difference between moist and dry region θ^*_{eb}. In this section, we show that the persistence enhancement due to convergence coupling is distinct from this effect.

The lagged correlation results for the THERMO and DCON setups are available in Figure 9. The wave persistence is indeed enhanced in the THERMO simulation with a weaker warm pool, but there are still important differences between the setups. The wave in the THERMO simulation shows a broader correlation structure in time near the $x_0 = 30,000$ km and it shows correlations with a westward propagating wave at a lag of 5 days. Qualitatively the correlation structure is similar to that seen in Figure 8.

The DCON simulation, on the other hand, shows a very localized wave which does not correlate with any westward waves. This mirrors the results in the previous section. Moreover, the wave shows strong lag correlations with an eastward traveling wave at $x = 0$ km, at a lag of 7.5 days. This eastward traveling wave is likely generated in the dry region by convergence due to dry gravity waves emanating from the CCW around $x = 30,000$ km. This reemergence of moist waves is not present in the THERMO simulations, and it is clear that the enhanced persistence via convergence coupling is a distinct effect.

3) Moisture budget

The differences between QE and CISK lies in relationships between the various terms in the column integrated moisture budget (Emanuel et al. 1994; Arakawa 2004). In the present context, this is given by (5), which we repeat here for convenience,

$$\frac{\partial \langle q \rangle}{\partial t} + \frac{\partial}{\partial x}\langle uq \rangle = -\frac{2\sqrt{2}}{\pi}P + \frac{D}{H_T}$$

Examining the lagged correlation structure of the various terms in the moisture budget also provides insight into the enhanced persistence of the CCWs. Specifically, the lagged cross-correlation of vertically integrated moisture convergence $\nabla \cdot \langle uq \rangle$ and precipitation P is revealing. Unlike, the wave propagation diagrams in Figure 8, this quantity is calculated for each spatial location separately, and is given by

$$\rho(x,t) = \mathrm{Corr}(\nabla \cdot \langle uq \rangle (x,t), P(x,t)). \tag{17}$$

Figure 10 contains this quantity for the standard THERMO and DCON simulations.

Both simulations have similar structure, with three general types of relationship between $\nabla \cdot \langle uq \rangle$ and P. First, moisture convergence is negatively correlated with precipitation in the warm pool region, which is a result of the heavy congestus and stratiform heating in this region. In the dry regions near 0 km, the moisture convergence and precipitation are positively correlated for several lags. Finally, the flank regions (e.g. 27000km) show an interesting regime where $\rho(x, \pm\tau) < 0$ for $\tau > .25$ days, but $\nabla \cdot \langle uq \rangle$ and P are positively correlated for shorter lags. This last moisture budget regime corresponds to the passage of a wave like that seen Figures 6, 7, and 8. For the current purposes, CISK is defined by a two way feedback between moisture convergence and precipitation. However, in the flank region regime, moisture convergence predicts total heating, but total heating is anticorrelated with precipitation for larger lags.

As the THERMO simulations show, even a QE-based scheme can have regions where the moisture budget shows some characteristics of CISK (e.g. 0 km), and other regions where surface fluxes are of primary importance (e.g. warm pool). Moreover, because the same three regimes are present in both the THERMO and DCON simulations, it is clear that the method of convergence coupling considered here does not fundamentally change the thermodynamics of the scheme. In other words, DCON does not act like the Kuo-like moisture-convergence closure that was criticized in (Emanuel et al. 1994). The DCON scheme simply alters the location of these three moisture budget regimes, and the flank region moisture budget regime covers a much larger swath of the domain (e.g. 25000 km to 35000 km). This is precisely the same region where the CCW propagation was enhanced (cf. Figure 8).

b. Congestus convergence coupled CCON

At this point, we digress to explore an interesting negative result. Namely, we claim that coupling congestus clouds to the convergence is highly *unrealistic*, and should be avoided in the development of prototype cumulus parameterizations. Given the results of Figures 2 and 3, one might naively expect that the CCON regime, which replaces the *moist* convergence mechanism with a *dry* convergence mechanism, to perform comparably to a deep-coupled regime. This is, however, not the case, because unlike the deep-coupled setup, the CCON setup shows strong sensitivities to the key parameters τ_w and R.

The CCON setup is overly sensitive to the convergence coupling strength parameter (τ_w). A fact that the climatology of u_1 available in Figure 11 clearly demonstrates. As τ_w is increased, the strengths of the mean circulation and the variability are noticeably decreased. The CCON parameterization appears to shut down the circulation for these large values of τ_w. One potential explanation for this malignant behavior can be seen be varying the parameter R.

The interaction radius (R) explicitly controls the scales over which the large-scale convergence field interacts with the grid-scale convection. Ideally, one would prefer the dynamics to internally set this scale. In other simulations (not shown), the DCON scheme was insensitive to this parameter. Moreover, convection in the warm pool region is essentially unaltered in the DCON simulation compared to the control (THERMO). On the other hand, convection in the warm pool region in the CCON simulation is strongly dependent on R.

In this section, we demonstrate the interaction radius sensitivity by performing numerical experiments for interaction radii $R = 80,\ 160,\ 240$, and 480 km with a fixed value $\tau_w = 10$ hours. The zoomed-in 15 day snapshots of the congestus cloud fractions (σ_c) shown in Figure 12 provide a possible explanation for this. Compared to the THERMO simulation, the cloud fractions are smaller overall, and show a noisier background state. In particular, the cloud fractions are slaved to dry waves that emanate from the larger CCWs and propagate with a speed of 25 m/s. These dry waves carry elevated cloud fractions which occasionally interact to produce large enough cloud fractions to initiate a large CCW. Both the dry and convectively coupled waves noticeably increase in horizontal extent (decrease wave number) with R.

These larger waves appear to interact more strongly with one another than with the mean circulation, which increases the variability, but decreases the strength of the climatological circulation. This profound sensitivity to the parameters R and τ_w reflects the explicit role convergence-coupling plays when attached to the formation of congestus clouds. In fact, this scheme shows evidence of grid-scale convection as R is decreased, which is a hallmark of CISK. This is in contrast to the attractive results seen above for the deep-convergence-coupled (DCON) formulation.

5. Conclusions

In this study, we have modified the stochastic multicloud model to include the non-local effects of convergence coupling. This is motivated by recent work showing the importance of the convergence coupling in column multicloud models run in a diagnostic setting (Peters et al. 2013; Dorrestijn et al. 2015). However, these diagnostic studies cannot address the dynamical criticisms of convergence coupling provided by (Emanuel et al. 1994) and others. The present study addresses these traditional criticisms by implementing convergence coupling in a fully prognostic spatially extended setting.

We conclude that the addition of convergence coupling does have beneficial effects if implemented in the correct way. To be specific, coupling the transition from congestus to deep clouds to both the large-scale convergence and local CAPE, enhances the persistence of convectively coupled waves in nonlinear idealized warm pool simulations. Because there is no rotation in the model, these waves are analogous to equatorial Kelvin waves in the real atmosphere. Therefore, the *soft* non-local convergence coupling presented here potentially describes the remarkable ability of atmospheric Kelvin waves to sometimes propagate unimpeded across the eastern Pacific and the Andes mountain range (Straub and Kiladis 2002; Kiladis et al. 2009).

This scheme also shows an attractive, but subtle, sensitivity to the convergence coupling strength (τ_w), which results in chaotic time-series with rich low-frequency content. This behavior likely results because the convergence-coupling enables a reciprocal interaction of dry and moist waves. The interaction of moist and dry waves is a well known mechanism to create "gregarious" multi-scale organized convection (Mapes 1993; Stechmann and Majda 2009). Moreover, it is desirable that the setup shows low sensitivity to the tuning parameter R, the interaction radius. Indeed, extreme sensitivity to this and other parameters is a key symptom of the degenerate congestus-convergence-coupled scheme. The latter serves as an example of how *not* to implement convergence coupling as shown in Section 4b.

The deep convergence coupled setup does not fundamentally alter the thermodynamics of convection compared to the original multicloud formulation. This form of non-local convergence coupling is not a moisture-convergence closure like the Kuo schemes, and it does not show unattractive CISK-like behavior, as shown in Section 4a. Indeed the current results complement the evidence that the transition from shallow to deep convection is promoted by vertical moisture transport (Hagos et al. 2014). On the other hand, coupling the congestus clouds to the convergence field shows unattractive characteristics reminiscent of CISK. This reflects the intuition that the formation of congestus clouds is driven boundary layer dynamics rather than the free tropospheric convergence field.

It is unknown how the addition of rotation and another horizontal spatial dimension will effect these results on non-local convergence coupling, so extending the present work to a more realistic atmospheric simulation is an interesting avenue of future research. There is existing work on implementing the stochastic multicoud model in a full atmospheric GCM (Ajayamohan et al. 2013, 2014; Deng et al. 2014; Peters et al. 2015) that can be leveraged for these purposes. Also, while the model studied here includes the effects of stratiform heating, the formation of stratiform clouds is not explicitly coupled to the winds in any way. Coupling the stratiform clouds to vertical velocity and/or shear in idealized Walker circulation simulations is another interesting research direction.

In summary, this paper indicates that non-local convergence coupling potentially plays an important role in mediating interactions between convection and a large-scale SST driven circulation. This mechanism is distinct from the wind induced surface heating mechanism. We stress here that in models with non-homogeneous SSTs, the relationships between terms in the moisture budget often depends on the region. In moist regions with high SST, surface heat fluxes can play a key role, but in drier/colder regions precipitation is frequently associated with large-scale moisture convergence. Coupling the transition from congestus to deep clouds appears to beneficially alter dynamics in these drier regions, while leaving convection in the moist regions largely untouched.

Acknowledgments. The authors thank Boualem Khouider for stimulating discussion on this subject and Olivier Pauluis for helping improve the presentation of these results. The research of A. J. M. is partially supported by the Office of Naval Research MURI award grant ONR-MURI N-000-1412-10912. Y. F. is a postdoctoral fellow supported through the above MURI award, and N.D.B. is supported as a graduate student on the MURI award.

References

Ajayamohan, R. S., B. Khouider, and A. J. Majda, 2013: Realistic initiation and dynamics of the madden-julian oscillation in a coarse resolution aquaplanet GCM. *Geophys. Res. Lett.*, **40 (23)**, 6252–6257, doi:10.1002/2013gl058187, URL http://dx.doi.org/10.1002/2013GL058187.

Ajayamohan, R. S., B. Khouider, and A. J. Majda, 2014: Simulation of monsoon intraseasonal oscillations in a coarse-resolution aquaplanet GCM. *Geophys. Res. Lett.*, **41 (15)**, 5662–5669, doi:10.1002/2014gl060662, URL http://dx.doi.org/10.1002/2014GL060662.

Arakawa, A., 2004: The cumulus parameterization problem: Past, present, and future. *J. Climate*, **17 (13)**, 2493–2525.

Arakawa, A., and W. H. Schubert, 1974: Interaction of a cumulus cloud ensemble with the large-scale environment, Part I. *J. Atmos. Sci.*, **31**, 674–701.

Betts, A. K., and M. J. Miller, 1986: A new convective adjustment scheme. Part II: Single column tests using GATE wave, BOMEX, ATEX and Arctic air-mass data sets. *Quarterly Journal of the Royal Meteorological Society*, **112 (473)**, 693–709.

Buizza, R., M. Miller, and T. N. Palmer, 1999: Stochastic representation of model uncertainties in the ECMWF Ensemble Prediction System. *Quarterly Journal of the Royal Meteorological Society*, **125**, 2887–2908.

Charney, J. G., and A. Eliassen, 1964: On the growth of the hurricane depression. *Journal of the Atmospheric Sciences*, **21 (1)**, 68–75.

Chevrotière, M. D. L., B. Khouider, and A. J. Majda, 2014: Calibration of the stochastic multicloud model using bayesian inference. *SIAM J. Sci. Comput.*, **36 (3)**, B538–B560, doi:10.1137/13094267x, URL http://dx.doi.org/10.1137/13094267X.

Crueger, T., B. Stevens, and R. Brokopf, 2013: The madden-julian oscillation in echam6 and the introduction of an objective mjo metric. *J. Climate*, **26 (10)**, 3241–3257, doi:10.1175/jcli-d-12-00413.1, URL http://dx.doi.org/10.1175/JCLI-D-12-00413.1.

Davies, L., C. Jakob, P. May, V. V. Kumar, and S. Xie, 2013: Relationships between the large-scale atmosphere and the small-scale convective state for darwin, australia. *Journal of Geophysical Research: Atmospheres*, **118 (20)**, 11,534–11,545, doi:10.1002/jgrd.50645, URL http://dx.doi.org/10.1002/jgrd.50645.

Del Genio, A. D., Y. Chen, D. Kim, and M.-S. Yao, 2012: The mjo transition from shallow to deep convection in cloudsat /calipso data and GISs GCM simulations. *J. Climate*, **25 (11)**, 3755–3770, doi:10.1175/jcli-d-11-00384.1, URL http://dx.doi.org/10.1175/JCLI-D-11-00384.1.

Deng, Q., B. Khouider, and A. J. Majda, 2014: The mjo in a coarse-resolution GCM with a stochastic multicloud parameterization. *J. Atmos. Sci.*, 140915145827003, doi:10.1175/jas-d-14-0120.1, URL http://dx.doi.org/10.1175/JAS-D-14-0120.1.

Dorrestijn, J., D. T. Crommelin, A. P. Siebesma, H. J. J. Jonker, and C. Jakob, 2015: Stochastic parameterization of convective area fractions with a multicloud model inferred from observational data. *J. Atmos. Sci.*, **72 (2)**, 854–869, doi:10.1175/jas-d-14-0110.1, URL http://dx.doi.org/10.1175/JAS-D-14-0110.1.

ECMWF, 2003: *Proceedings ECMWF/CLIVAR Workshop on Simulation and Prediction of Intraseasonal variability with Emphasis on the MJO*, 3–6 November.

Emanuel, K. A., J. David Neelin, and C. S. Bretherton, 1994: On large-scale circulations in convecting atmospheres. *Quarterly Journal of the Royal Meteorological Society*, **120 (519)**, 1111–1143, doi:10.1002/qj.49712051902, URL http://dx.doi.org/10.1002/qj.49712051902.

Frenkel, Y., B. Khouider, and A. J. Majda, 2013: Stochastic and deterministic multicloud parameterizations for tropical convection. *Climate Dynamics*, **41**, 1527–1551.

Frenkel, Y., A. J. Majda, and B. Khouider, 2012: Using the stochastic multicloud model to improve tropical convective parameterization: A paradigm example. *J. Atmos. Sci.*, **69 (3)**, 1080–1105.

Frierson, D. M., A. J. Majda, and O. M. Pauluis, 2004: Large scale dynamics of precipitation fronts in the tropical atmosphere: A novel relaxation limit. *Commun. Math. Sci.*, **2 (4)**, 591–626, URL http://projecteuclid.org/euclid.cms/1109885499.

Gardiner, C., 2009: *Stochastic methods : a handbook for the natural and social sciences*. Springer, Berlin Heidelberg.

Gillespie, D. T., 1975: An exact method for numerically simulating the stochastic coalescence process in a cloud. *J. Atmos. Sci.*, **32**, 1977–1989.

Gillespie, D. T., 1977: Exact stochastic simulation of coupled chemical reactions. *The Journal of Physical Chemistry*, **81 (25)**, 2340–2361.

Grabowski, W. W., 2001: Coupling cloud processes with the large-scale dynamics using the cloud-resolving convection parameterization. *J. Atmos. Sci.*, **58 (9)**, 978–997.

Grabowski, W. W., 2004: An improved framework for superparameterization. *J. Atmos. Sci.*, **61 (15)**, 1940–1952.

Grabowski, W. W., and M. W. Moncrieff, 2001: Large-scale organization of tropical convection in two-dimensional explicit numerical simulations. *Q.J Royal Met. Soc.*, **127 (572)**, 445–468, doi:10.1002/qj.49712757211, URL http://dx.doi.org/10.1002/qj.49712757211.

Grabowski, W. W., and P. K. Smolarkiewicz, 1999: CRCP: A Cloud Resolving Convection Parameterization for modeling the tropical convecting atmosphere. *Physica D Nonlinear Phenomena*, **133**, 171–178.

Hagos, S., Z. Feng, K. Landu, and C. N. Long, 2014: Advection, moistening, and shallow-to-deep convection transitions during the initiation and propagation of madden-julian oscillation. *Journal of Advances in Modeling Earth Systems*, **6 (3)**, 938–949, doi:10.1002/2014ms000335, URL http://dx.doi.org/10.1002/2014MS000335.

Hendon, H. H., and B. Liebmann, 1994: Organization of convection within the Madden–Julian oscillation. *J. GEOPHYS. RES.*, **99**, 8073–8084.

Johnson, R. H., T. M. Rickenbach, S. A. Rutledge, P. E. Ciesielski, and W. H. Schubert, 1999: Trimodal characteristics of tropical convection. *Journal of Climate*, **12 (8)**, 2397–2418.

Katsoulakis, M. A., A. J. Majda, and D. G. Vlachos, 2003a: Coarse-grained stochastic processes and monte carlo simulations in lattice systems. *Journal of Computational Physics*, **186**, 250 – 278.

Katsoulakis, M. A., A. J. Majda, and D. G. Vlachos, 2003b: Coarse-grained stochastic processes for microscopic lattice systems. *Proceedings of the National Academy of Sciences of the United States of America*, **100**, 782–787.

Khouider, B., 2014: A coarse grained stochastic multi-type particle interacting model for tropical convection: Nearest neighbour interactions. *Communications in Mathematical Sciences*, **8**, 1379–1407.

Khouider, B., j. Biello, and A. J. Majda, 2010: A stochastic multicloud model for tropical convection. *Comm. Math. Sci.*, **8 (1)**, 187–216.

Khouider, B., and A. J. Majda, 2005a: A non oscillatory balanced scheme for an idealized tropical climate model; Part I: Algorithm and validation. *Theoretical and Computational Fluid Dyn.*, **19**, 331–354.

Khouider, B., and A. J. Majda, 2005b: A non oscillatory balanced scheme for an idealized tropical climate model; Part II: Nonlinear coupling and moisture effects. *Theoretical and Computational Fluid Dyn.*, **19**, 355–375.

Khouider, B., and A. J. Majda, 2006a: Multicloud convective parametrizations with crude vertical structure. *Theor. Comp. Fluid Dyn.*, **20 (1)**, 351–375.

Khouider, B., and A. J. Majda, 2006b: A simple multicloud parametrization for convectively coupled tropical waves. Part I: Linear analysis. *J. Atmos. Sci.*, **63 (2)**, 1308–1323.

Khouider, B., and A. J. Majda, 2007: A simple multicloud parametrization for convectively coupled tropical waves. Part II: Nonlinear simulations. *J. Atmos. Sci.*, **64**, 381–400.

Khouider, B., and A. J. Majda, 2008a: Equatorial convectively coupled waves in a simple multicloud model. *J. Atmos. Sci.*, **65**, 3376–3397.

Khouider, B., and A. J. Majda, 2008b: Multicloud models for organized tropical convection: Enhanced congestus heating. *J. Atmos. Sci.*, **65**, 897–914.

Khouider, B., A. J. Majda, and M. A. Katsoulakis, 2003: Coarse grained stochastic models for tropical convection and climate. *Proc. Nat. Acad. Sci.*, **100**, 11 941–11 946, doi:10.1073/pnas.1634951100.

Khouider, B., A. St-Cyr, A. J. Majda, and J. Tribbia, 2011: The mjo and convectively coupled waves in a coarse-resolution GCM with a simple multicloud parameterization. *J. Atmos. Sci.*, **68 (2)**, 240–264, doi:10.1175/2010jas3443.1, URL http://dx.doi.org/10.1175/2010JAS3443.1.

Kiladis, G. N., M. C. Wheeler, P. T. Haertel, K. H. Straub, and P. E. Roundy, 2009: Convectively coupled equatorial waves. *Reviews of Geophysics*, **47 (2)**, doi:10.1029/2008rg000266, URL http://dx.doi.org/10.1029/2008RG000266.

Kuo, H. L., 1974: Further studies of the parameterization of the influence of cumulus convection on large-scale flow. *J. Atmos. Sci.*, **31**, 1232–1240.

Lau, W. K. M., and D. E. Waliser, 2005: *Intraseasonal Variability in the Atmosphere-Ocean Climate System*. Springer-Verlag, 436 pp.

Lin, J., and J. D. Neelin, 2003: Toward stochastic deep convective parameterization in general circulation models. *Geophys. Res. Lett.*, **30 (4)**, 1162.

Lin, J.-L., and Coauthors, 2006: Tropical intraseasonal variability in 14 IPCC AR4 climate models. Part I: Convective signals. *Journal of Climate*, **19 (12)**, 2665–2690.

Lindzen, R. S., 1974: Wave-CISK in the tropics. *Journal of the Atmospheric Sciences*, **31 (1)**, 156–179, doi:10.1175/1520-0469(1974)031⟨0156:wcitt⟩2.0.co;2, URL http://dx.doi.org/10.1175/1520-0469(1974)031⟨0156:WCITT⟩2.0.CO;2.

Majda, A. J., 2007: Multiscale models with moisture and systematic strategies for superparameterization. *J. Atmos. Sci.*, **64 (7)**, 2726–2734.

Majda, A. J., C. Franzke, and B. Khouider, 2008: An applied mathematics perspective on stochastic modelling for climate. *Philosophical Transactions of the Royal Society A: Mathematical, Physical and Engineering Sciences*, **366 (1875)**, 2427–2453.

Majda, A. J., and B. Khouider, 2002: Stochastic and mesoscopic models for tropical convection. *Proceedings of the National Academy of Science*, **99**, 1123–1128.

Majda, A. J., and S. N. Stechmann, 2008: Stochastic models for convective momentum transport. *Proceedings of the National Academy of Sciences*, **105 (46)**, 17 614–17 619.

Manabe, S., J. Smagorinsky, and R. F. Strickler, 1965: Simulated climatology of a general circulation model with a hydrologic cycle1. *Monthly Weather Review*, **93 (12)**, 769–798.

Mapes, B. E., 1993: Gregarious tropical convection. *J. Atmos. Sci.*, **50 (13)**, 2026–2037, doi:10.1175/1520-0469(1993)050⟨2026:gtc⟩2.0.co;2, URL http://dx.doi.org/10.1175/1520-0469(1993)050⟨2026:GTC⟩2.0.CO;2.

Mapes, B. E., 2000: Convective inhibition, subgrid-scale triggering energy, and stratiform instability in a toy tropical wave model. *J. Atmos. Sci.*, **57 (10)**, 1515–1535.

Moncrieff, M., M. Shapiro, J. Slingo, and F. Molteni, 2007: Collaborative research at the intersection of weather and climate. *WMO Bulletin*, **56**, 204–211.

Moncrieff, M. W., and E. Klinker, 1997: Organized convective systems in the tropical western Pacific as a process in general circulation models: A TOGA COARE case-study. *Quarterly Journal of the Royal Meteorological Society*, **123**, 805–827.

Nakazawa, T., 1974: Tropical super clusters within intraseasonal variation over the western pacific. *J. Meteorol. Soc. Japan*, **66**, 823–839.

Palmer, T. N., 2001: A nonlinear dynamical perspective on model error: A proposal for non-local stochastic-dynamic parametrization in weather and climate prediction models. *Quarterly Journal of the Royal Meteorological Society*, **127**, 279–304.

Peters, K., C. Jakob, L. Davies, B. Khouider, and A. J. Majda, 2013: Stochastic behavior of tropical convection in observations and a multicloud model. *J. Atmos. Sci.*, **70**, 3556– 3575.

Peters, K., C. Jakob, and B. Mobis, 2015: The stochastic multicloud model (smcm) as part of an operational convection parameterisation in a comprehensive gcm. *EGU General Assembly*.

Plant, R. S., and G. C. Craig, 2008: A stochastic parameterization for deep convection based on equilibrium statistics. *Journal of the Atmospheric Sciences*, **65 (1)**, 87–105, doi:10.1175/2007jas2263.1, URL http://dx.doi.org/10.1175/2007JAS2263.1.

Randall, D., M. Khairoutdinov, A. Arakawa, and W. Grabowski, 2003: Breaking the cloud parameterization deadlock. *Bulletin of the American Meteorological Society*, **84 (11)**, 1547–1564.

Scinocca, J. F., and N. A. McFarlane, 2004: The variability of modeled tropical precipitation. *J. Atmos. Sci.*, **61**, 1993–2015.

Slawinska, J., O. Pauluis, A. J. Majda, and W. W. Grabowski, 2014a: Multi-scale interactions in an idealized walker circulation: Simulations with sparse space-time superparameterization. *Mon Weather Review*, **In Press**.

Slawinska, J., O. Pauluis, A. J. Majda, and W. W. Grabowski, 2014b: Multiscale Interactions in an Idealized Walker Circulation: Mean Circulation and Intraseasonal Variability. *Journal of Atmospheric Sciences*, **71**, 953–971.

Slingo, J. M., and Coauthors, 1996: Intraseasonal oscillations in 15 atmospheric general circulation models: results from an AMIP diagnostic subproject. *Climate Dynamics*, **12**, 325–357.

Stechmann, S. N., and A. J. Majda, 2009: Gravity waves in shear and implications for organized convection. *J. Atmos. Sci.*, **66 (9)**, 2579–2599, doi:10.1175/2009jas2976.1, URL http://dx.doi.org/10.1175/2009JAS2976.1.

Straub, K. H., and G. N. Kiladis, 2002: Observations of a convectively coupled kelvin wave in the eastern pacific itcz. *J. Atmos. Sci.*, **59 (1)**, 30–53, doi:10.1175/1520-0469(2002)059⟨0030:ooacck⟩2.0.co;2, URL http://dx.doi.org/10.1175/1520-0469(2002)059⟨0030:OOACCK⟩2.0.CO;2.

Suhas, E., and G. J. Zhang, 2014: Evaluation of trigger functions for convective parameterization schemes using observations. *Journal of Climate*, **27 (20)**, 7647–7666, doi:10.1175/jcli-d-13-00718.1, URL http://dx.doi.org/10.1175/JCLI-D-13-00718.1.

Wheeler, M., and G. N. Kiladis, 1999: Convectively coupled equatorial waves: Analysis of clouds and temperature in the wavenumber-frequency domain. *J. Atmos. Sci.*, **56 (3)**, 374–399.

Xing, Y., A. J. Majda, and W. W. Grabowski, 2009: New efficient sparse space–time algorithms for superparameterization on mesoscales. *Monthly Weather Review*, **137 (12)**, 4307–4324.

Zhang, C., 2005: Madden–Julian oscillation. *Reviews of Geophysics*, **43**, RG2003.

LIST OF TABLES

Table 1. Default constants and parameters common to all multicloud simulations discussed in this report. The horizontal rules divide deterministic, stochastic parameters from FMK13, convergence coupling parameters, and numerical parameters, respectively. Largely reproduced from FMK13. 37

Table 2. Summary of important diagnostic quantities in (1)-(7). 38

Table 3. Stochastic transition rates with multiplicative convergence coupling. Compare to Table 2 from FMK13. 39

Parameter	Value	Description
$h_b/H_m/H_T$	500 m / 5 km/ 16 km	ABL depth/ average depth of the mid-troposphere/ Free troposphere depth
Q_{R1}	1 K/day	First baroclinic radiative cooling rate
Q_{R2}	Determined at RCE	Second baroclinic radiative cooling rate
ξ_s/ξ_c	0.4/0	Stratiform/Congestus contribution to first baroclinic mode
$\tilde{Q}$	0.9	Background moisture stratification
$\tilde{\lambda}/\tilde{\alpha}$	0.8/0.1	Coefficient of u_2 in linear / nonlinear moisture convergence
m_0	Determined at RCE	Large-scale background downdraft velocity scale
μ	0.25	Contribution of convective downdrafts to D
α_s/α_c	0.25/ 0.1	Stratiform/Congestus adjustment coefficient
τ_R/τ_D	75 days / 50 days	Rayleigh drag / Newtonian cooling time scale
τ_s/τ_c	3 hours / 2 hour	Stratiform /Congestus adjustment time scale
τ_{conv}	2 hours	Convective time scale
τ_e	Determined by RCE	Surface evaporation time scale
$\bar{Q}$	Determined at RCE	Bulk convective heating at RCE
$\bar{\theta}_{eb}-\bar{\theta}_{em}$	11 K	Mean (RCE) Dryness of the atmosphere
θ^-/θ^+	10 K /20 K	Deterministic moisture switch threshold values
A/B	1/0	Deterministic moisture switch parameters
a_1/a_2	0.50 / 0.50	Relative contribution of θ_{eb} / q to deep convection
a_0/a_0'	2 / 1.5	Dry convective buoyancy frequency in deep/congestus heating equations.
γ_2/γ_2'	0.1 / 2	Relative contribution of θ_2 to deep /congestus heating
α_2	0.1	Relative contribution of θ_2 to θ_{em}
C_d	0.001	Surface drag coefficient
u_0	2 m/s	Strength of turbulent fluctuations
$\bar{\alpha}$	$\approx$ 15 K	Unit scale of temperature
$CAPE_0$	400 J/Kg	Reference values of CAPE
T_0	30 K	Reference values of dryness
τ_{01}	1 hr	Timescale for formation of congestus clouds
τ_{02}	3 hr	Timescale for formation of deep clouds
τ_{12}	1 hr	Timescale for congestus-to-deep transition
τ_{23}	3 hr	Timescale for deep-to-stratiform transition
τ_{10}	1 hr	Timescale for death of congestus clouds
τ_{20}	3 hr	Timescale for death of deep clouds
τ_{30}	3 hr	Timescale for death of stratiform clouds
τ_W	10 hours	Strength of convergence coupling
R	240 km	Radius of convergence coupling
$\overline{W}$	$-\log(.8)$	RCE convergence propensity
z_{01}	2 km	Height of convergence-driven formation of congestus heating
z_{02}	4 km	Height of convergence-driven formation of deep heating
z_{12}	8 km	Height of convergence-driven transition from congestus to deep heating
L	40,000 km	Length of domain
Δx	40 km	Grid spacing
Δt	0.5 minutes	Maximum time step
n_x	1000	Number of grid cells
ℓ^2	$900 = 30^2$	Number of stochastic sites

TABLE 1. Default constants and parameters common to all multicloud simulations discussed in this report. The horizontal rules divide deterministic, stochastic parameters from FMK13, convergence coupling parameters, and numerical parameters, respectively. Largely reproduced from FMK13.

Description	Expression
Midlevel θ_e	$\theta_{em} = q + \frac{2\sqrt{2}}{\pi}(\theta_1 + \alpha_2\theta_2)$
Precipitation	$P = H_d + \xi_s H_s + \xi_c H_c$
Downdrafts	$D = m_0(1+\mu(H_s - H_c)/Q_{R01})^+(\theta_{eb} - \theta_{em})$
Evaporation	$\frac{E}{h_b} = \frac{1}{\tau_e}(\theta^*_{eb} - \theta_{eb})$
Radiation	$\text{Rad}_1 = Q_{R01} - \frac{\theta_1}{\tau_D}$, and $\text{Rad}_2 = Q_{R02} - \frac{\theta_2}{\tau_D}$
CAPE	$CAPE = \overline{CAPE} + R(\theta_{eb} - \gamma(\theta_1 + \gamma_2\theta_2))$
Lower level CAPE	$CAPE_l = \overline{CAPE} + R(\theta_{eb} - \gamma(\theta_1 + \gamma_2'\theta_2))$
Deep heating	$H_d = \left[\sigma_d \bar{Q} + \frac{\sigma_d}{\bar{\sigma}_d \tau_c^0}(a_1\theta_{eb} + a_2 q - a_0(\theta_1 + \gamma_2\theta_2))\right]^+$
Congestus heating	$H_c = \sigma_c \frac{\alpha_c \bar{\alpha}}{H_m}\sqrt{CAPE_l^+}$

TABLE 2. Summary of important diagnostic quantities in (1)-(7).

Transition rate	Time scale(h)
Formation of congestus	$R_{01} = \frac{1}{\tau_{01}}\Gamma(C_l)\Gamma(D)\Gamma(W_{01})$
Decay of congestus	$R_{10} = \frac{1}{\tau_{10}}\Gamma(D)$
Conversion of congestus to deep	$R_{12} = \frac{1}{\tau_{12}}\Gamma(C)(1-\Gamma(D))\Gamma(W_{12})$
Formation of deep	$R_{02} = \frac{1}{\tau_{02}}\Gamma(C)(1-\Gamma(D))\Gamma(W_{02})$
Conversion of deep to stratiform	$R_{23} = \frac{1}{\tau_{23}}$
Decay of deep	$R_{20} = \frac{1}{\tau_{20}}(1-\Gamma(C))$
Decay of stratiform	$R_{30} = \frac{1}{\tau_{30}}$

TABLE 3. Stochastic transition rates with multiplicative convergence coupling. Compare to Table 2 from FMK13.

LIST OF FIGURES

Fig. 1. Schematic of the convergence coupling formulation in terms of velocity convergences at different height levels z_{ij}. In this schematic, the $1 \to 2$ transition from congestus to deep clouds is coupled to the convergence at a greater height than the $0 \to 2$ formation of deep clouds because the former develops from the moistening of the mid-troposphere by congestus clouds. Stratiform clouds are not coupled directly to the non-local convergence or the local thermodynamic state. Adapted from KM06a. 42

Fig. 2. u_1 anomaly Hovmoller diagrams of the last 200 days of simulations of the three stochastic setups. The mixed non-local convergence-coupled setups (CCON and DCON) have more chaotic and variable time signals than the thermodynamic-only (THERMO) simulation. . . . 43

Fig. 3. u_1 climatological mean spatial pattern for the three stochastic setups. The DCON simulation has slightly higher mean velocities near the flanks of the warm pool. The congestus coupling reduces the strength of the mean circulation compared to THERMO. 44

Fig. 4. u_1 anomaly Hovmoller diagrams for the thermodynamic-only (THERMO) simulation, and the deep-convergence-coupled (DCON) simulations with the convergence coupling strength τ_w increasing in each panel from left to right. The tendency of convectively coupled waves to depart the warm pool at regular 12 day intervals in precisely alternating directions is increasingly disrupted for large values of τ_w. Moreover, in the $\tau_w = 10$ simulation the dominate waves depart the warm pool at longer 25-day interval (days 820-900), and there is change in regime towards smaller waves around day 930. 45

Fig. 5. u_1 climatology for varying τ_w for the deep-convergence coupled (DCON) simulations. The thermodynamic-only (THERMO) simulation is plotted for comparison (blue). $\tau_w = 1, 10, 100$, and 1000 are gray with lighter shades indicating larger τ_w. The DCON variability is everywhere larger than the THERMO variability, with an especially strong effect outside the warm pool. The variability tends to increase for larger convergence-coupling strength τ_w. 46

Fig. 6. A strong convectively coupled wave for the deep-convergence-coupled (DCON) regime. A 30 day snapshot of the moisture field q including the temporal mean is plotted. As seen below in Figure 7, the wave changes vertical structure as it passes from the edge of the warm pool (A) into the dry region (B), and the phase speed reduces from 13.5 m/s to 9.5 m/s. This wave interacts with the warm pool region via fast-moving dry waves, typical examples of which are marked using dashed lines. 47

Fig. 7. Vertical and horizontal wave structure for the convectively coupled wave shown in Figure 6. These plots are averaged along the labeled lines in that figure. Inside the warm pool (A), the wave shows strong congestus heating, which transforms into deep heating outside of the warm-pool (B). A reduction in phase-speed from 13.5 to 9.5 m/s accompanies this transition. . 48

Fig. 8. The lagged correlation between congestus heating at $x = 30,000$ km and deep heating elsewhere in the domain for $A_{SST} = 5$ K. This is a signature of large convectively coupled waves which feature a robust transition from congestus to deep heating. The DCON wave propagates much more coherently into the dry region. 49

Fig. 9. Like Figure 8 but for a warm-pool amplitude of $A_{SST} = 4.5$ K. 50

Fig. 10. Lagged correlation between moisture convergence and precipitation. Unlike Figure 8, the autocorrelation function for each spatial location is calculated independently. The key fea-

ture is that the region where moisture convergence predicts precipitation is much larger in the DCON simulation. 51

Fig. 11. Climatology for u_1 for CCON simulations with varying τ_w for fixed $R = 240$ km. Blue is the control THERMO simulation. CCON is run with τ_w = 10, 100, and 300, which are plotted in gray with lighter shades indicating higher τ_w. 52

Fig. 12. σ_c Hovmoller diagrams for the congestus convergence-coupled (CCON) setup for various interaction radii R with fixed $\tau_w = 10$ hr. The upper left panel shows the control THERMO simulation, while the other three panels contain the CCON simulations. In the CCON panels, fast moving second baroclinic dry waves with a phase speed of approximately 25 m/s propagate away from slower moving convectively coupled waves. The horizontal scale of both the dry and convectively coupled waves increases notably with R. 53

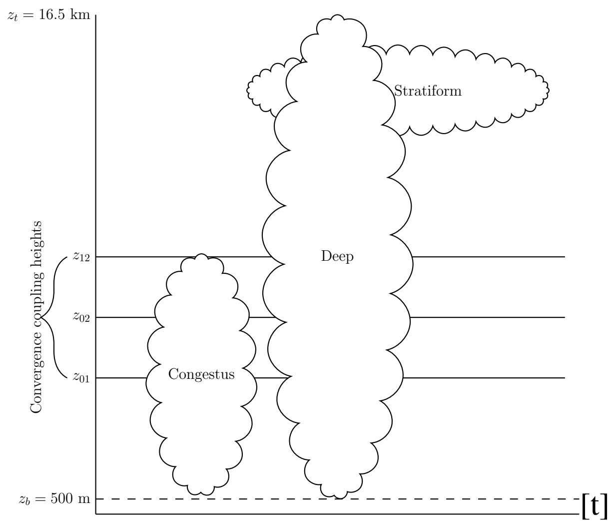

FIG. 1. Schematic of the convergence coupling formulation in terms of velocity convergences at different height levels z_{ij}. In this schematic, the $1 \rightarrow 2$ transition from congestus to deep clouds is coupled to the convergence at a greater height than the $0 \rightarrow 2$ formation of deep clouds because the former develops from the moistening of the mid-troposphere by congestus clouds. Stratiform clouds are not coupled directly to the non-local convergence or the local thermodynamic state. Adapted from KM06a.

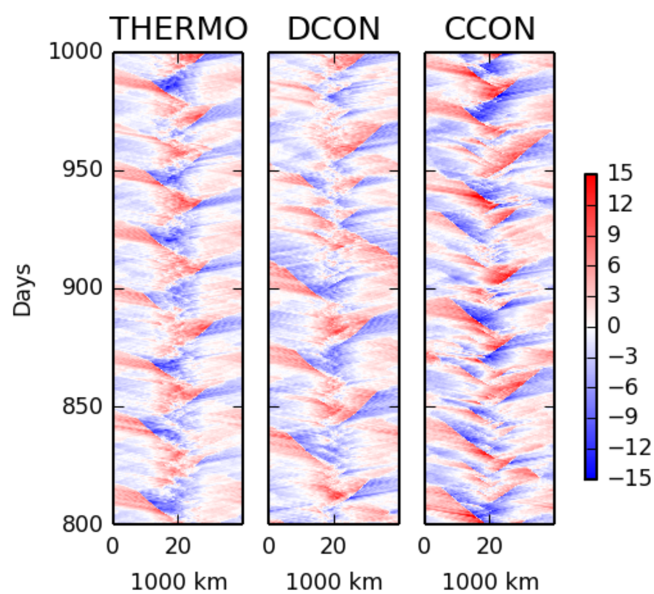

FIG. 2. u_1 anomaly Hovmoller diagrams of the last 200 days of simulations of the three stochastic setups. The mixed non-local convergence-coupled setups (CCON and DCON) have more chaotic and variable time signals than the thermodynamic-only (THERMO) simulation.

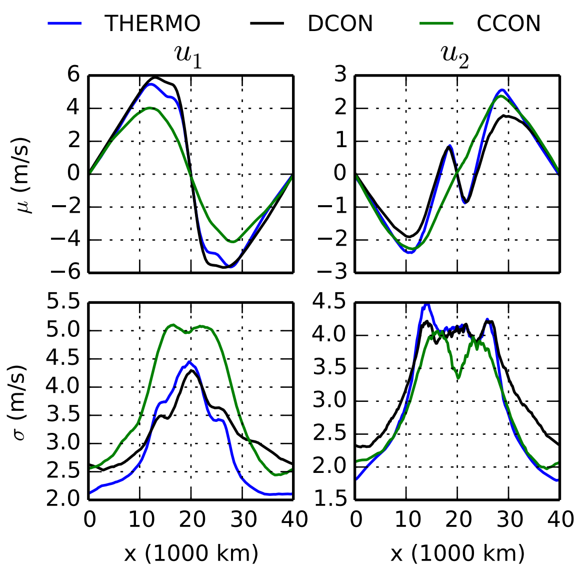

825 FIG. 3. u_1 climatological mean spatial pattern for the three stochastic setups. The DCON simulation has slightly higher mean velocities near the flanks of the warm pool. The congestus coupling reduces the strength of the mean circulation compared to THERMO.

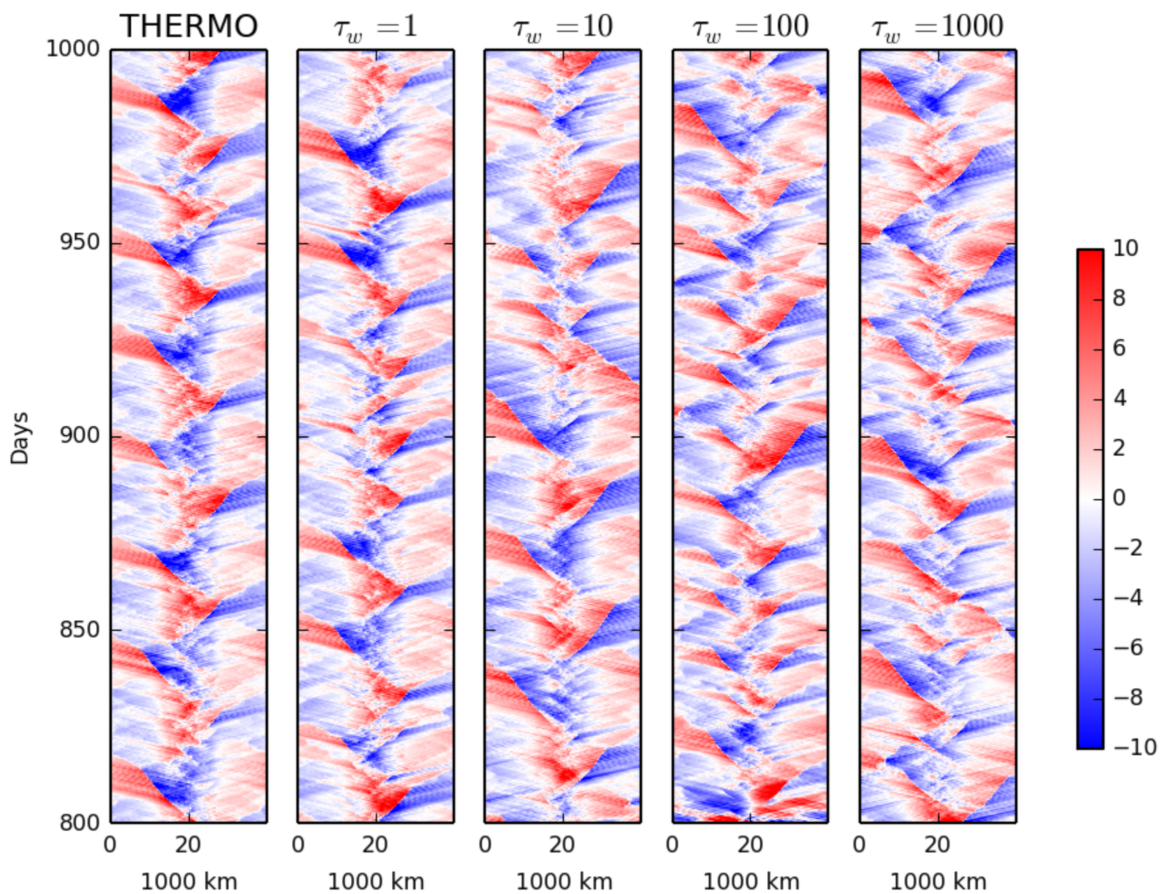

FIG. 4. u_1 anomaly Hovmoller diagrams for the thermodynamic-only (THERMO) simulation, and the deep-convergence-coupled (DCON) simulations with the convergence coupling strength τ_w increasing in each panel from left to right. The tendency of convectively coupled waves to depart the warm pool at regular 12 day intervals in precisely alternating directions is increasingly disrupted for large values of τ_w. Moreover, in the $\tau_w = 10$ simulation the dominate waves depart the warm pool at longer 25-day interval (days 820-900), and there is change in regime towards smaller waves around day 930.

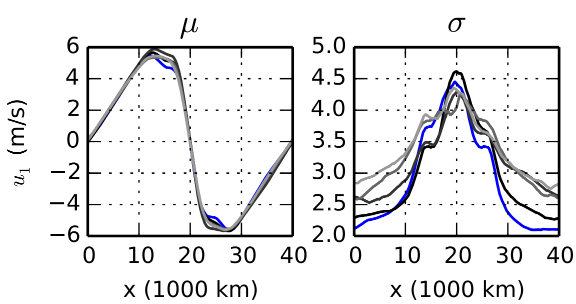

FIG. 5. u_1 climatology for varying τ_w for the deep-convergence coupled (DCON) simulations. The thermodynamic-only (THERMO) simulation is plotted for comparison (blue). $\tau_w = 1, 10, 100$, and 1000 are gray with lighter shades indicating larger τ_w. The DCON variability is everywhere larger than the THERMO variability, with an especially strong effect outside the warm pool. The variability tends to increase for larger convergence-coupling strength τ_w.

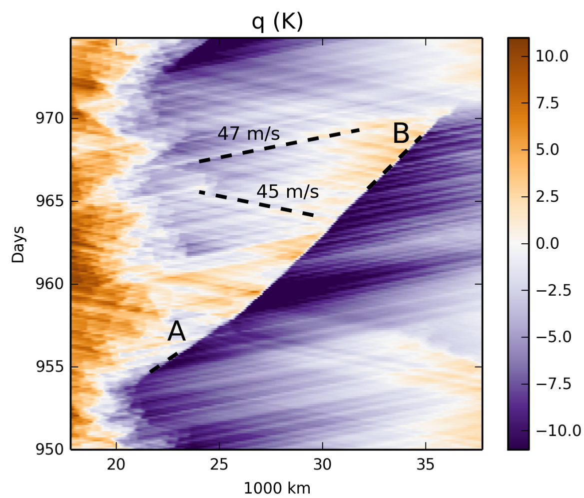

FIG. 6. A strong convectively coupled wave for the deep-convergence-coupled (DCON) regime. A 30 day snapshot of the moisture field q including the temporal mean is plotted. As seen below in Figure 7, the wave changes vertical structure as it passes from the edge of the warm pool (A) into the dry region (B), and the phase speed reduces from 13.5 m/s to 9.5 m/s. This wave interacts with the warm pool region via fast-moving dry waves, typical examples of which are marked using dashed lines.

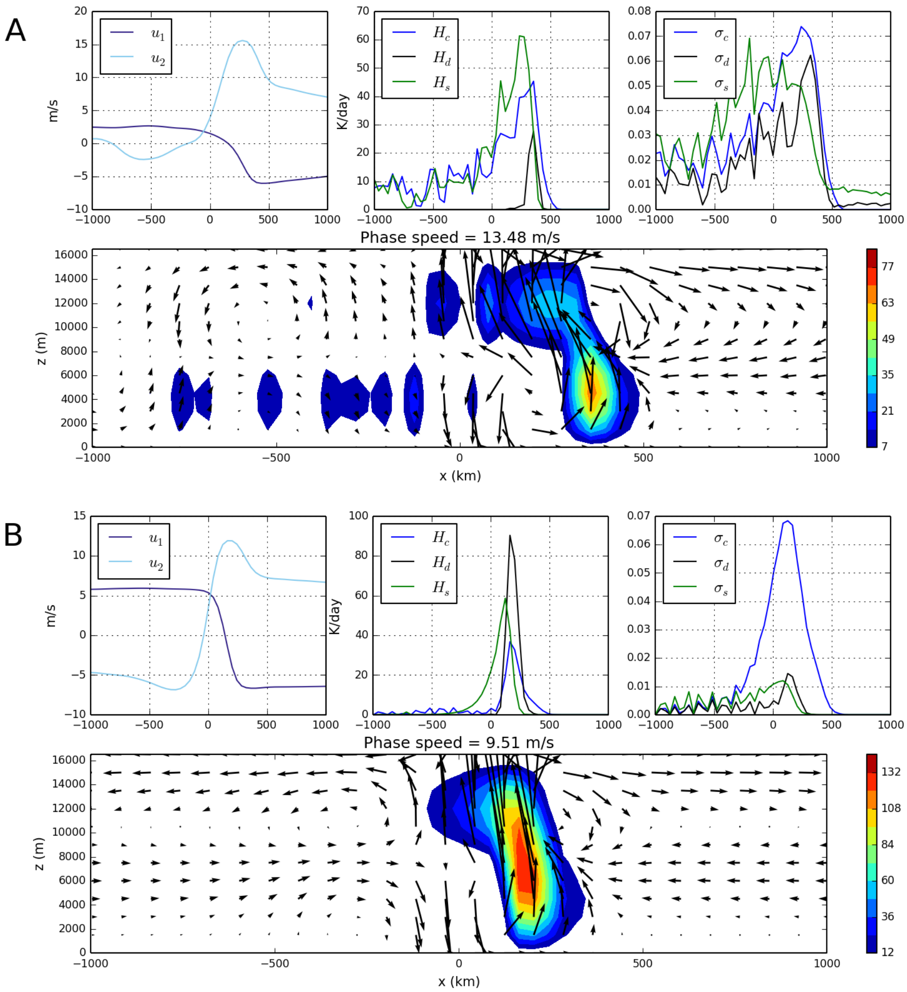

FIG. 7. Vertical and horizontal wave structure for the convectively coupled wave shown in Figure 6. These plots are averaged along the labeled lines in that figure. Inside the warm pool (A), the wave shows strong congestus heating, which transforms into deep heating outside of the warm-pool (B). A reduction in phase-speed from 13.5 to 9.5 m/s accompanies this transition.

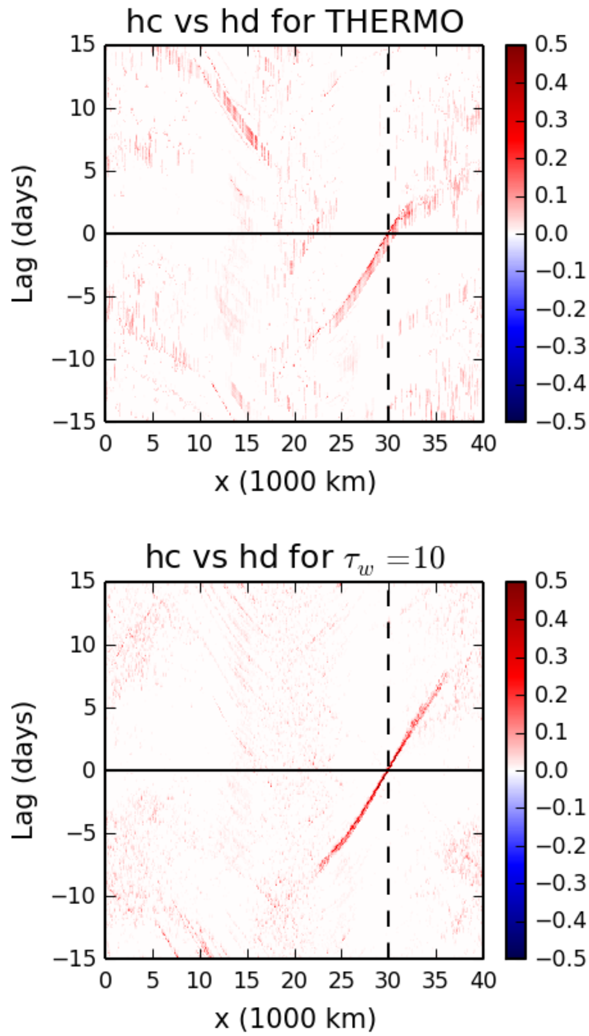

FIG. 8. The lagged correlation between congestus heating at $x = 30,000$ km and deep heating elsewhere in the domain for $A_{SST} = 5$ K. This is a signature of large convectively coupled waves which feature a robust transition from congestus to deep heating. The DCON wave propagates much more coherently into the dry region.

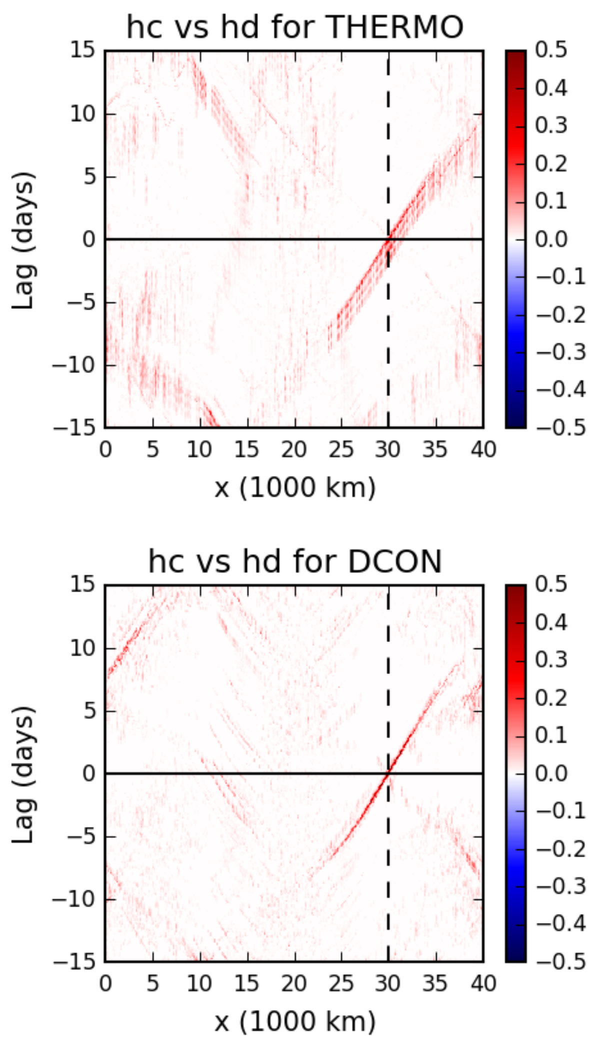

FIG. 9. Like Figure 8 but for a warm-pool amplitude of $A_{SST} = 4.5$ K.

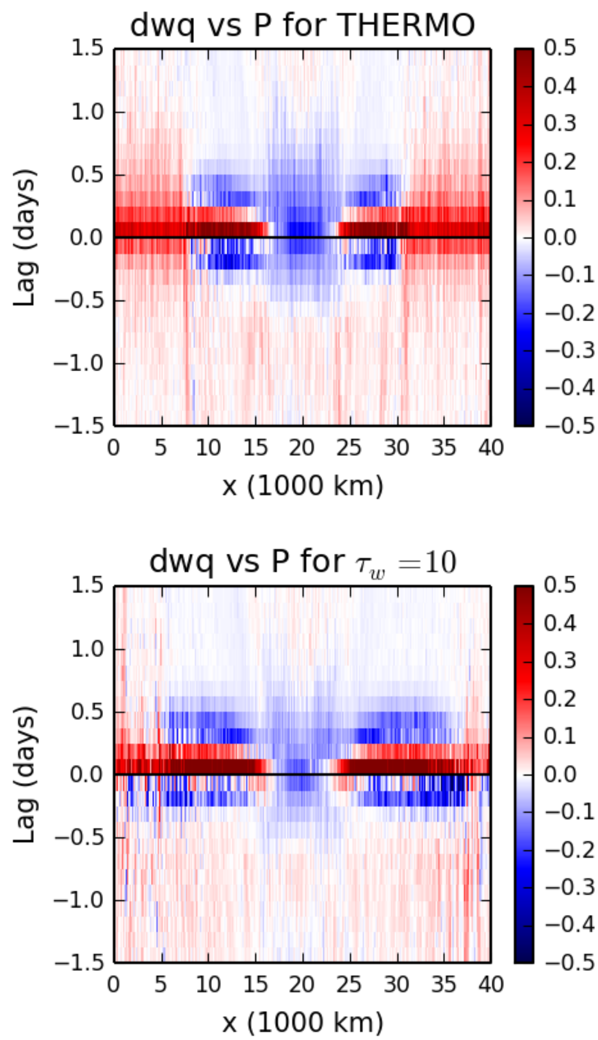

FIG. 10. Lagged correlation between moisture convergence and precipitation. Unlike Figure 8, the autocorrelation function for each spatial location is calculated independently. The key feature is that the region where moisture convergence predicts precipitation is much larger in the DCON simulation.

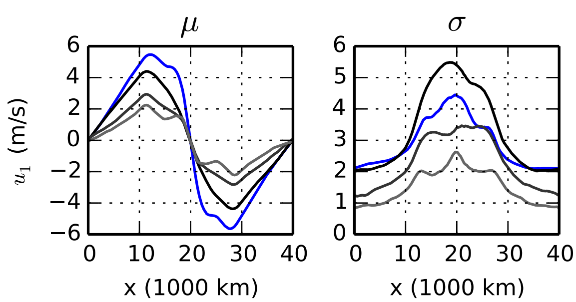

FIG. 11. Climatology for u_1 for CCON simulations with varying τ_w for fixed $R = 240$ km. Blue is the control THERMO simulation. CCON is run with $\tau_w = 10$, 100, and 300, which are plotted in gray with lighter shades indicating higher τ_w.

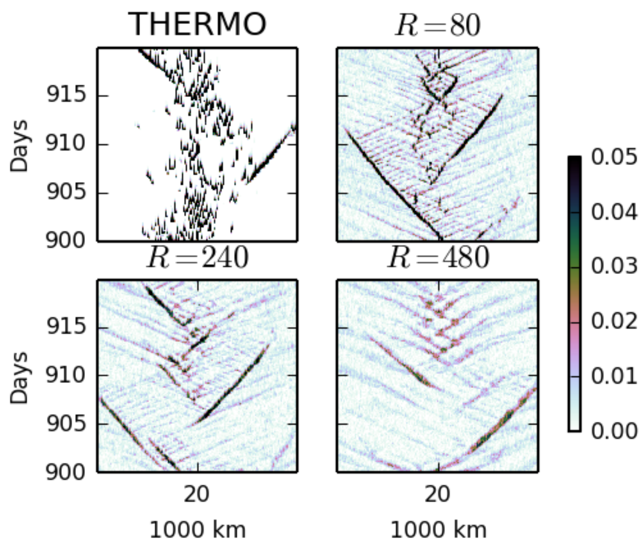

FIG. 12. σ_c Hovmoller diagrams for the congestus convergence-coupled (CCON) setup for various interaction radii R with fixed $\tau_w = 10$ hr. The upper left panel shows the control THERMO simulation, while the other three panels contain the CCON simulations. In the CCON panels, fast moving second baroclinic dry waves with a phase speed of approximately 25 m/s propagate away from slower moving convectively coupled waves. The horizontal scale of both the dry and convectively coupled waves increases notably with R.